STScI | SPACE TELESCOPE SCIENCE INSTITUTE

JWST TECHNICAL REPORT

Title: Astrometric accuracy of the JWST calibration field catalog examined with the first Gaia data release	Doc #: JWST-STScI-005492, SM-12 Date: 24 January 2017 Rev: -
Authors: Phone: 410 Johannes Sahlmann 338-2407	Release Date: 2 May 2017

1 Abstract

We investigate the astrometric agreement of sources in common between the JWST calibration field catalog on the basis of Hubble Space Telescope (HST) ACS observations and the first data release (DR1) of the Gaia mission. We find significant offsets, rotation, scale differences, skew, and higher-order geometric distortions between both catalogs. The modeled scale difference corresponds to field-dependent offsets with an RMS across the field of 1.8 mas, which in combination with on-axis skew and off-axis skew (0.4 mas RMS) and higher-order terms (RMS of 0.5 mas in X and 1.0 mas in Y) accumulate in RMS to 2.0 mas in X and 1.7 mas in Y. Terms that are not global offsets, rotation, or scale accumulate to an RMS of 0.5 mas in X and 0.9 mas in Y. Because the HST catalog will serve as astrometric reference for JWST, these terms will have to be accounted for when determining the field-distortion of JWST science instruments to an accuracy of about 2 mas or better. The residual dispersion between both catalogs is dominated by the internal proper motion dispersion of the LMC stars, a situation that could be mitigated with an additional HST observation of the field and when the second Gaia data release becomes available. Under the assumption that Gaia data are accurate and distortion-free, we present a correction to the JWST calibration field astrometric catalog.

2 Introduction

The JWST calibration field located in the LMC and the southern continuous viewing zone is of fundamental importance for JWST Science Operations (Diaz-Miller 2007, van der Marel et al. 2007). It will be observed intensively during JWST commissioning and repeatedly during the nominal mission. In particular, the calibration field will serve for the determination and monitoring of the geometric distortion of the telescope and science instruments (SI) (e.g. Anderson 2016).

The field was characterized astrometrically (Anderson & Diaz 2011) and photometrically (Anderson 2008) with HST and complemented with Very Large Telescope near-infrared observations. The Gaia DR1 (Gaia Collaboration et al. 2016a, Gaia Collaboration et al. 2016b) offers the opportunity to perform an independent verification of the astrometry.

2.1 Purpose of the study

This report addresses the question *How accurate is the HST astrometric catalog of the first JWST standard astrometric field?* with the help of Gaia DR1 astrometry. We are not directly verifying

a JWST requirement, but the results are relevant for various applications of the calibration field catalog, including the verification of certain requirements as discussed below.

2.2 Requirement on JWST field distortion uncertainty

The Level 3 requirement on field distortion uncertainty is ([SOC-2686], Section 3.4.3.2.5 of JWST-STSCI-000046 and [DMS-268], Section 3.2.1.5 of JWST-STScI-002249):

> "The DMS shall calibrate the field mapping of the SI coordinates relative to standard astrometric fields so that after calibration, the field distortion uncertainty within any SI and the guider does not exceed 0.005 arcsec, 1 sigma per axis."

Interpretation: It is understood that this requirement does not concern the accuracy of the *standard astrometric fields*/catalogs themselves, but rather the precision in a differential sense with which SI coordinates can be mapped to a given catalog of the observed calibration field, e.g. to a local local v2/v3 frame.

It is also understood that *field distortion* refers to displacements of star positions that cannot be modeled with two-dimensional polynomial terms that correspond to global offsets or a global rotation. It does include terms corresponding to a global scale, an on-axis skew, and off-axis skew, and all significant higher-order terms. This understanding may differ from the convention followed for HST, where global offsets, global rotation, and in particular global scale are considered *calibrations* and not *distortions.* To facilitate the interpretation of our results, we will report figures that relate to either convention.

The JWST requirements on global offset and global rotation are addressed in the SI-FGS requirements DMS-267 (SOC-3399) and DMS-265 (SOC-3402) discussed in JWST-STScI-004996.

Anderson (2016) has performed a general validation that the JWST field distortion uncertainty requirement above can be met for all SI and the guider in terms of guide-star availability and the properties of the star field (number, density, brightness) that allow to solve for the polynomial of the required degree (4 or 5), which provides the field distortion mapping with a precision of better than 5 mas per axis.

Here we undertake a complementary study of the astrometric accuracy of the HST calibration field catalog with the help of Gaia DR1.

3 Data selection and catalog crossmatch

The HST Catalog MASTER.ISO.XYVJHKRD was retrieved on 6 January 2017 from http://www.stsci.edu/~jayander/JWST_CALIBFIELD/ [1]. All Gaia sources included in DR1 and located within 0.06 degrees of the field center were retrieved from the Gaia Archive Core System located at ESA's European Space Astronomy Centre using pygacs (https://github.com/Johannes-Sahlmann/pygacs), a TAP interface to that archive in python, on 30 November 2016.

To retain high-fidelity Gaia sources, we discarded sources that had large positional uncertainties,

[1] Note that an earlier version of the catalog did not provide RA/Dec values with sufficient numerical resolution to perform this study, since they were provided only as a qualitative reference. Consequently, a new version of the catalog has been generated that preserves the full accuracy of the catalog in the RA/Dec values.

large excess noise, or indications of duplicity by imposing the following criteria on DR1 catalog fields: (duplicated_source == 0 & astrometric_excess_noise <=2.0 & astrometric_excess_noise_sig <= 10 & dec_error <= 5 & ra_error <= 5).

In the HST catalog we removed sources with V magnitudes (vcal) > 23, because those are beyond the faint limit of Gaia.

We crossmatched the two resulting catalogs within a search radius of 0.15 arcsecond and discarded any source that had multiple matches. We also discarded outliers in terms of angular-, RA-, and Dec-separation that appeared beyond three times the distributions' standard deviation from the median. This yields 2076 sources, shown in red in Figure 2. Their magnitude distributions in the HST and Gaia bands are shown in Figure 1. To further increase the fidelity of the crossmatched stars, we discarded 14 stars that have magnitude differences between Gaia and HST of $G–V < –0.4$ or $G–V > 2$. Finally, after a first full analysis the modeling residuals in Y/Dec were dominated by a non-Gaussian tail of outliers. We therefore discarded 42 additional stars that had residual amplitudes in Y/Dec larger than 3 times the RMS of 2.9 mas when fitting a polynomial of degree=3. This resulted in a final sample of 2020 crossmatched stars.

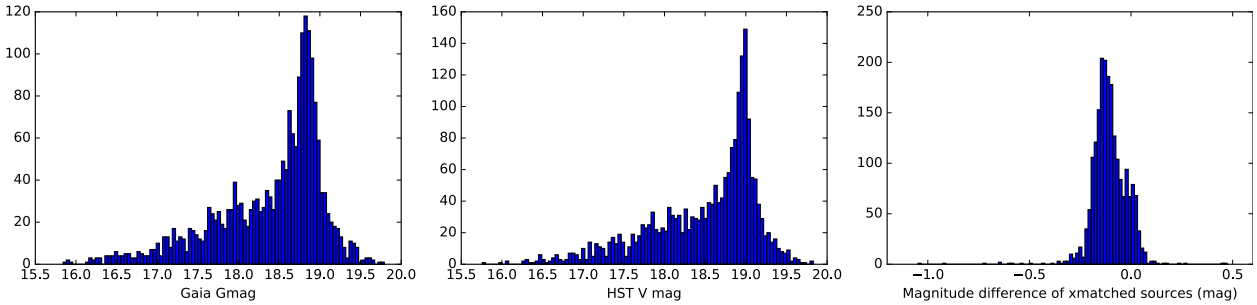

Figure 1: Gaia magnitudes (left), HST V magnitude (centre), and their difference distribution (right).

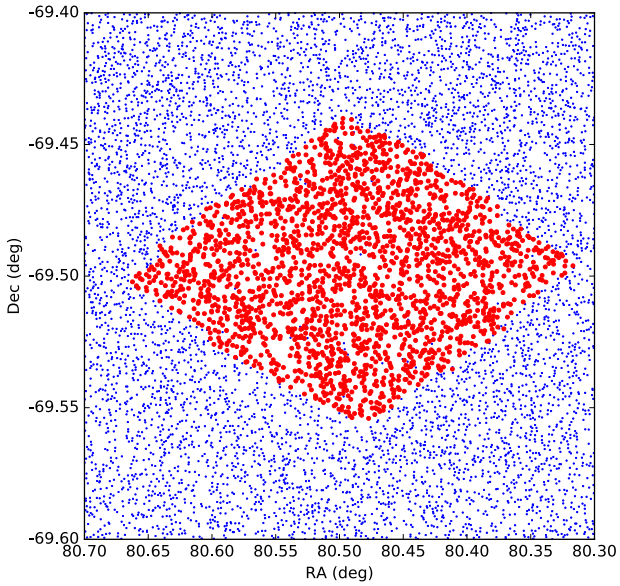

Figure 2: Crossmatched sources (red) and other Gaia sources (blue) in the vicinity of the calibration field.

4 Mapping the catalogs and the distortion

To map the catalogs we performed a tangent-plane projection to the X-Y-plane about the reference point (RA = 80.48878755, Dec = –69.49867070) with a scale factor that allows us to work in units of milli-arcsecond (mas). The source positions in X,Y and their uncertainties were fed into a fitting routine that derives the parameters of a two-dimensional polynomial that corresponds to the spatial mapping between both catalogs.

4.1 Polynomial fit

The general form of the commonly used bivariate polynomial is

$$x_{i,E} - x_{0,E} = {}^{\{x\}}A_0 + \sum_{l=1}^{k/2-1} \sum_{\substack{\alpha,\beta=0,\\ \alpha+\beta=l}}^{l} {}^{\{x\}}A_l^{\alpha,\beta}(x_{i,R} - x_{0,R})^{\alpha}(y_{i,R} - y_{0,R})^{\beta}$$

$$y_{i,E} - y_{0,E} = {}^{\{y\}}A_0 + \sum_{l=1}^{k/2-1} \sum_{\substack{\alpha,\beta=0,\\ \alpha+\beta=l}}^{l} {}^{\{y\}}A_l^{\alpha,\beta}(x_{i,R} - x_{0,R})^{\alpha}(y_{i,R} - y_{0,R})^{\beta}$$

where $x_{i,R}$, $y_{i,R}$ are the coordinates in the reference frame (here Gaia) of source *i*. $x_{i,E}$, $y_{i,E}$ are the coordinates in the evaluation frame, i.e. the catalog that is being solved for (here HST). The subscript 0 indicates the reference position. A_l are the polynomial coefficients that represent the free parameters of the system of equations.

Internally, we adopted the mode parameter *k*, introduced by Lazorenko & Lazorenko (2004) for the modeling of atmospheric image motion in ground-based narrow-field astrometry, to indicate the degree of the polynomial. A polynomial with mode *k* has a degree $d = k/2–1$ and $Nparam = k*(k+2)/8$ free parameters, where the degree indicates the highest total degree of the X/Y-terms. The two systems of equations in X and Y are solved independently, thus there are 2**Nparam* parameters in total. For convenience, we will list *d* alongside *k*.

Table 1: Mode, degree, and free parameters of the polynomial

Mode *k*	Degree *d*	Number of parameters *Nparam*
2	0	1
4	1	3
6	2	6
8	3	10
10	4	15
12	5	21
14	6	28

This model is linear in the coefficients and can therefore be solved uniquely by matrix inversion. The direct solution has the shortcoming that it only considers uncertainties in the dependent variables, i.e. the positional uncertainties in the evaluation frame. Uncertainties in the independent variables (positions in the reference frame) cannot be accounted for. We will refer

to the results of this method as the *direct solution*.

We also implemented a solution that is based on a python implementation of the mpfit code (kmpfit), and accounted for the uncertainties in the independent variables by using the effective variance method[2]. This solution is not direct but obtains the best-fit parameters using a Levenberg-Marquardt algorithm, which we fed with starting values given by the best-fit parameters of the direct solution. We will refer to this method as the *complete solution*.

4.2 Positional uncertainties in the HST and Gaia catalogs

The HST catalog of the JWST calibration field does not contain individual astrometric uncertainties, but it has been shown that relative positions are good to about 1 mas (Anderson & Diaz 2011).

Gaia DR1 lists a median astrometric uncertainty of 0.37 mas in RA and 0.78 mas in Dec for the 2020 sources in common with the HST catalog and used here.

When obtaining the complete solution, we found reduced χ^2 values systematically larger than one. We therefore set the astrometric uncertainty of the HST catalog globally to 2 mas, which brought the reduced χ^2 close to unity. This procedure may compensate for proper motion dispersion of the field and potential errors in the Gaia or HST astrometry as well. In practice its effect on the results is negligible.

4.3 Identification of significant modes

Naturally, an increase in the polynomial mode will lead to smaller residuals and better χ^2 because there are more free parameters. Fitting polynomials with arbitrarily high degree is undesirable and it is therefore necessary to identify the highest significant mode for a particular dataset. Because our model is linear and the residuals are quasi-normally distributed (indicating quasi-Gaussian errors, see Figure 6), we can use the F-test of additional model parameters to address this issue. Given two models with different numbers of free parameters and the corresponding χ^2 values, the F-test yields the probability that the simpler model is true by evaluating the improvement in χ^2 in relation to the number of additional free parameters. The χ^2 values are computed with the nominal uncertainties in the variables and no rescaling is applied.

We identified the highest significant mode by requiring that the F-test yield a probability >0.0027 (hence imposing a significance criterion at roughly 3 sigma) in both X- and Y-coordinate fits, which is the case for k=8 (d=3) as can be seen in Table 2. Whereas the residual RMS does not seem to decrease substantially, the F-test tells us that the k=8 model is a significantly better fit than the k=6 (d=2) model. We will therefore report the results of the fit with a polynomial of degree=3, complemented by results obtained with degree=1 because those have an intuitive interpretation.

Table 2 shows that the six-parameter model corresponding to a degree=1 polynomial is not sufficient to map the two catalogs because there is a significant improvement in the fit quality

[2] The effective variance is the sum of the variance in the dependent variable and the derivative of the model function multiplied by the variance in the independent variable, see the high-level description at https://www.astro.rug.nl/software/kapteyn/kmpfittutorial.html - fitting-data-when-both-variables-have-uncertainties.

when including higher-order terms.

Table 2: Residuals and F-test probability as a function of polynomial mode. The F-test of additional model parameters yields the probability that the model with mode *k* is true compared to the mode=*k*+2 model.

Mode	Degree	Direct solution				Complete solution			
		RMS (mas)		F-test probability		RMS (mas)		F-test probability	
k	*d*	X	Y	X	Y	X	Y	X	Y
4	1	1.835	2.513	2.25e-22	2.03e-44	1.835	2.514	2.28e-24	6.22e-48
6	2	1.789	2.388	1.22e-02	2.83e-06	1.789	2.388	6.41e-03	2.93e-07
8	3	1.783	2.369	5.88e-02	5.05e-03	1.783	2.370	6.38e-02	8.67e-03
10	4	1.778	2.359	3.05e-01	3.85e-01	1.779	2.360	2.18e-01	1.61e-01
12	5	1.775	2.356	8.55e-01	1.04e-01	1.775	2.357	7.21e-01	1.75e-01

5 Results

Figure 3 shows the differences between the catalog positions, which are dominated by a global offset. When correcting for the offset, a positive rotation becomes apparent (rotation angle measured from North to East), i.e. the HST catalog is rotated eastward relative to the Gaia catalog.

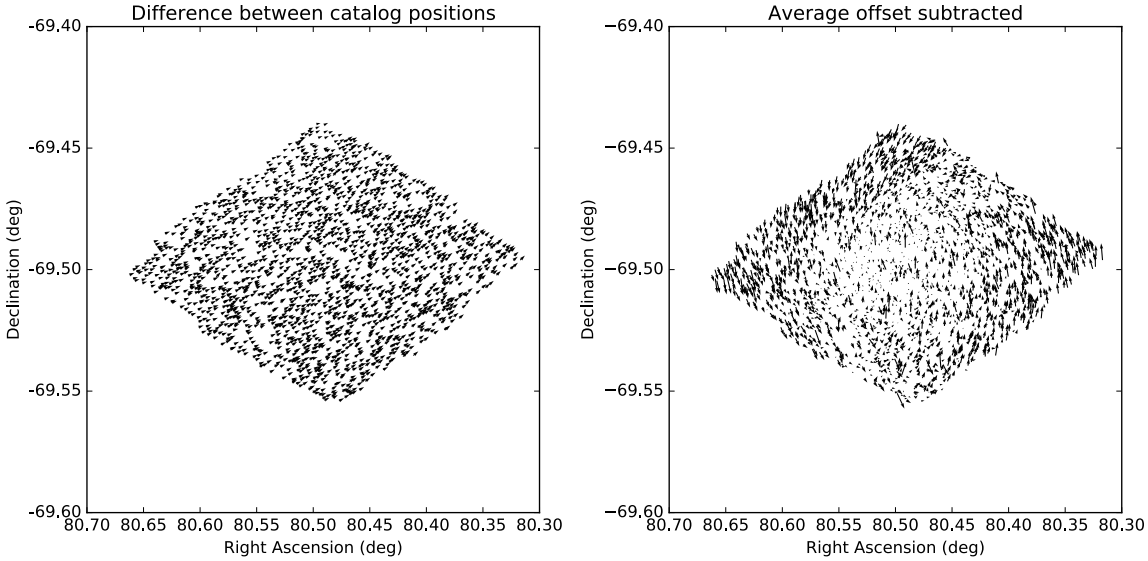

Figure 3: Position differences between the two catalogs (left, dominated by offsets) and after subtraction of the global offsets (right).

5.1 Mode *k*=4, polynomial degree *d* = 1

This mode has six free parameters that can be converted to yield shift in X and in Y, scale in X and in Y, and rotation in X and in Y, where the latter two can also be expressed as a global rotation and a skew, defined as the difference between rotation in X and in Y. Alternatively, we can convert the latter four parameters into a global scale, a global rotation, an on-axis skew (i.e. the scale variation between X and Y), and an off-axis skew term (i.e. the non-perpendicularity

between the X and Y axis), a parametrisation often used in the HST context (see e.g. Anderson 2007).

Let the partial derivatives be $b = \frac{\partial x_E}{\partial x_R}, c = \frac{\partial x_E}{\partial y_R}, e = \frac{\partial y_E}{\partial x_R}, f = \frac{\partial y_E}{\partial y_R}$, then the scale in X is defined as $scale_X = \sqrt{b^2 + c^2}$ and the scale in Y is $scale_Y = \sqrt{e^2 + f^2}$. For the present first-order polynomial, the partial derivatives correspond to $b = A_{1,X}, c = A_{2,X}, \ e = A_{1,Y}, \ f = A_{2,Y}$. Table 3 shows the values of the parameters discussed above and the prescriptions of how to compute them.

Table 3: Converted coefficients of the *k*=4/*d*=1 polynomial fit. The 'sigma' columns indicate the standard uncertainties rescaled to yield chi^2=1.

Parameter	Value	sigma	Unit	Comment
Shift in X	-79.691	0.041	mas	$A_{0,X}$
Shift in Y	21.973	0.056	mas	$A_{0,Y}$
Rotation in X	0.00218	0.00003	deg	$\mathrm{rot_x} = \arctan2(-e, b)$
Rotation in Y	0.00210	0.00003	deg	$\mathrm{rot_y} = \arctan2(c, f)$
Scale in X	0.9999789	0.0000004		$\sqrt{b^2 + c^2}$
Scale in Y	0.9999839	0.0000006		$\sqrt{e^2 + f^2}$
Rotation	0.00214	0.00002	deg	$(rot_x + rot_y)/2$
Skew	-0.00008	0.00004	deg	$rot_y - rot_x$
Global Rotation	0.00214	0.00002	deg	$\arctan2(c - e, b + f)$
Global Scale	0.9999814	0.0000004		$\sqrt{bf - ce}$
On-axis Skew	-2.50e-06	3.84e-07		$(b - f)/2$
Off-axis Skew	-7.11e-07	3.67e-07		$(c + e)/2$

This model quantifies the global rotation between both catalogs to +7.71 ± 0.08 arcsecond. It indicates a significant on-axis skew term and a marginally significant off-axis skew term. The residuals show a dependence on position in the field, in particular in the Y-coordinate (Figure 4).

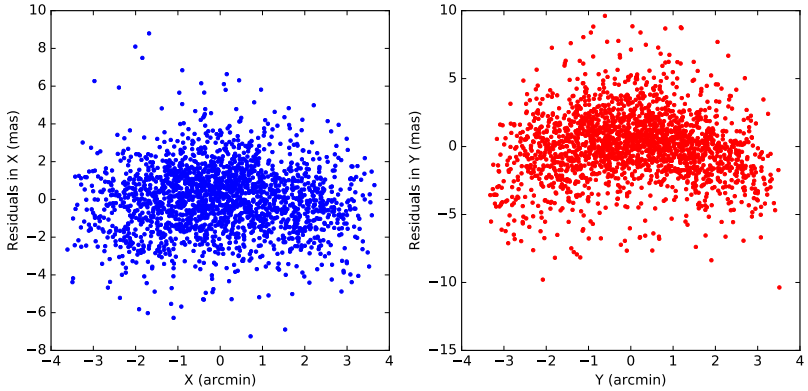

Figure 4: Residuals in X (left) and Y (right) as a function of position in X and Y, respectively, for *k*=4 (*d*=1).

5.2 Mode *k*=8, polynomial degree = 3

This is the model we adopted to characterize the geometric distortion between the HST and Gaia catalogs. Table 4 lists the polynomial coefficients and their uncertainties for the direct and the complete solution, which generally are in very good agreement when considering the uncertainties. In the following discussion, we will report the results of the direct solution when not specified otherwise.

Table 4: Polynomial coefficients for *k*=8 / *d*=3. The coefficient order conforms with the JWST Science Instrument Aperture File (SIAF) convention (Cox & Lallo 2017). The 'sigma' columns indicate the standard uncertainties rescaled to yield chi^2=1.

		Direct solution				Complete solution			
		X		Y		X		Y	
Reduced chi^2		0.80		1.41		0.70		0.99	
Param	Term	value	sigma	value	sigma	value	sigma	value	sigma
A_0	1	-79.812	0.076	22.760	0.101	-79.809	0.088	22.756	0.0940
A_1	x	0.999978	0.000001	-0.000032	0.000002	0.999978	0.000001	-0.000032	0.000001
A_2	y	0.000040	0.000001	0.999982	0.000002	0.000039	0.000001	0.999981	0.000002
A_3	x^2	-1.65e-11	4.54e-12	-6.70e-12	6.04e-12	-1.70e-11	5.24e-12	-6.29e-12	5.64e-12
A_4	x*y	-3.83e-11	7.41e-12	-3.83e-12	9.85e-12	-3.81e-11	8.64e-12	-1.38e-12	9.26e-12
A_5	y^2	3.08e-11	4.83e-12	-9.04e-11	6.41e-12	3.22e-11	5.63e-12	-8.80e-11	6.03e-12
A_6	x^3	3.13e-17	4.50e-17	-1.99e-16	5.99e-17	3.86e-17	5.20e-17	-2.13e-16	5.58e-17
A_7	x^2*y	-1.08e-16	1.00e-16	2.66e-16	1.33e-16	-1.04e-16	1.17e-16	2.71e-16	1.25e-16
A_8	x*y^2	1.94e-16	1.05e-16	-6.94e-16	1.39e-16	2.13e-16	1.21e-16	-6.80e-16	1.30e-16
A_9	y^3	-1.48e-16	4.93e-17	9.68e-17	6.55e-17	-1.49e-16	5.73e-17	9.25e-17	6.12e-17

5.2.1 Residuals

The residual RMS is 1.783 mas in X and 2.369 mas in Y. The residual distribution is close to Gaussian and does not show a dependence on location in the field, see Figure 5, Figure 6, and Figure 7.

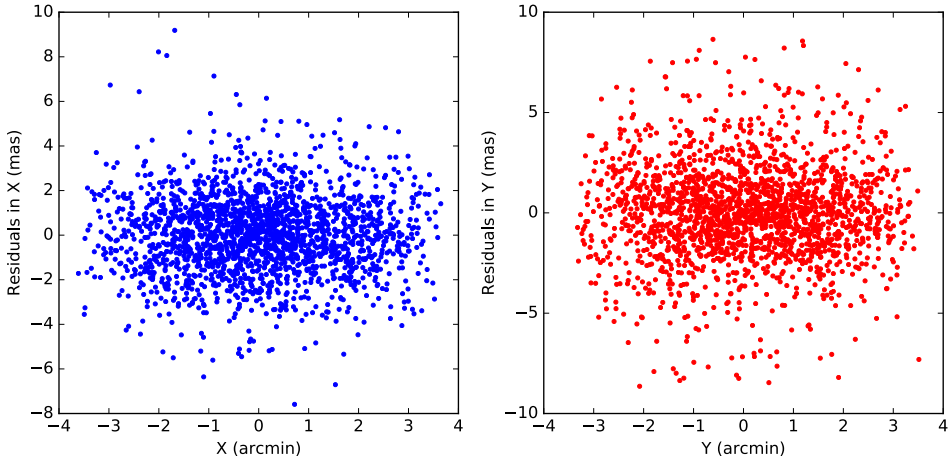

Figure 5: Residuals in X (left) and Y (right) as a function of position in X and Y, respectively, for *k*=8.

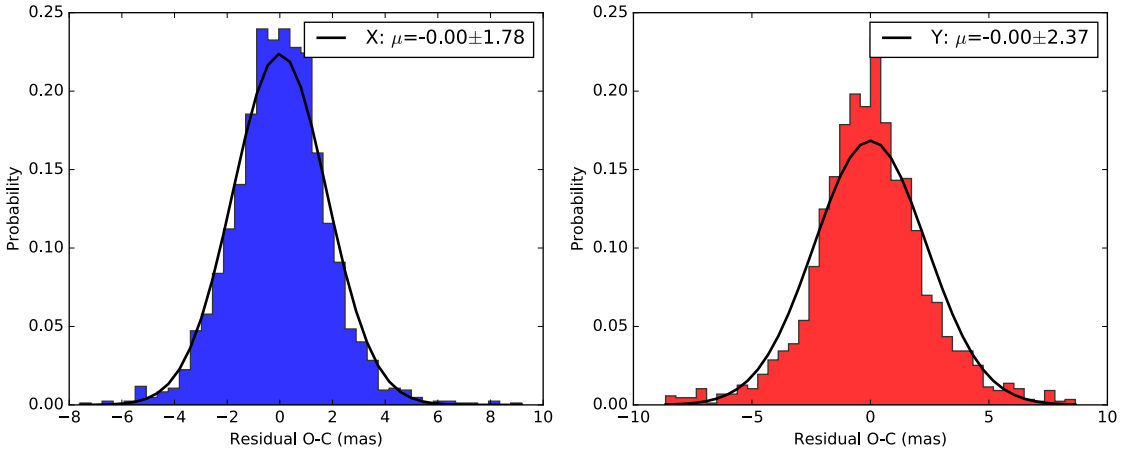

Figure 6: Residual histogram in X (blue) and Y (red) for *k*=8. The corresponding Gaussian models are drawn.

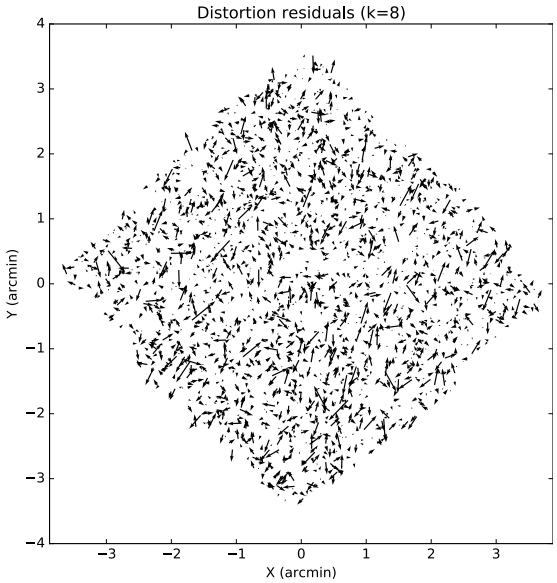

Figure 7: Residuals in X and Y as a function of position in the field. The longest arrow indicates a residual amplitude of 11.8 mas.

Check with the JWST SOCCER Database at: https://soccer.stsci.edu
To verify that this is the current version.

5.2.2 Coefficients corresponding to a first-degree polynomial

In Table 5 we report the first three polynomial coefficients (A_0,A_1,A_2) converted to the parameters introduced in Section 5.1. Their values are different from Table 3 because the higher-order terms were considered in this solution. For instance, the global rotation is now +7.36 ± 0.2 arcsecond.

Table 5: Converted first-degree coefficients of the *k*=8/*d*=3 polynomial fit.

Parameter	Value	sigma	Unit
Shift in X	-79.812	0.076	mas
Shift in Y	22.761	0.101	mas
Rotation in X	0.001821	0.000088	deg
Rotation in Y	0.002267	0.000068	deg
Scale in X	0.9999778	0.0000012	
Scale in Y	0.9999816	0.0000016	
Rotation	0.0020440	0.0000555	deg
Skew	0.0004459	0.0001109	deg
Global Rotation	0.0020440	0.0000555	deg
Global Scale	0.9999797	0.0000010	
On-axis Skew	-1.88e-06	1.01e-06	
Off-axis Skew	3.89e-06	9.67e-07	

The parameter A_0 corresponds to the global offset between the catalogs. Because of the scaling we chose, its value corresponds to units of mas. The HST – Gaia offset is –79.812 ± 0.076 mas in X (or RA[3]) and +22.761 ± 0.101 mas in Y (or Dec), thus the HST catalog is shifted west and North relative to the Gaia catalog.

The contributions of the A_1 and A_2 terms are visualized in Figure 8, where we distinguished global scale, global rotation, and on-axis and off-axis skew terms as defined in Section 5.1.

[3] When discussing offsets in RA, we refer to angular separation, i.e. $\Delta\alpha^* = \Delta\alpha \cos(\delta)$.

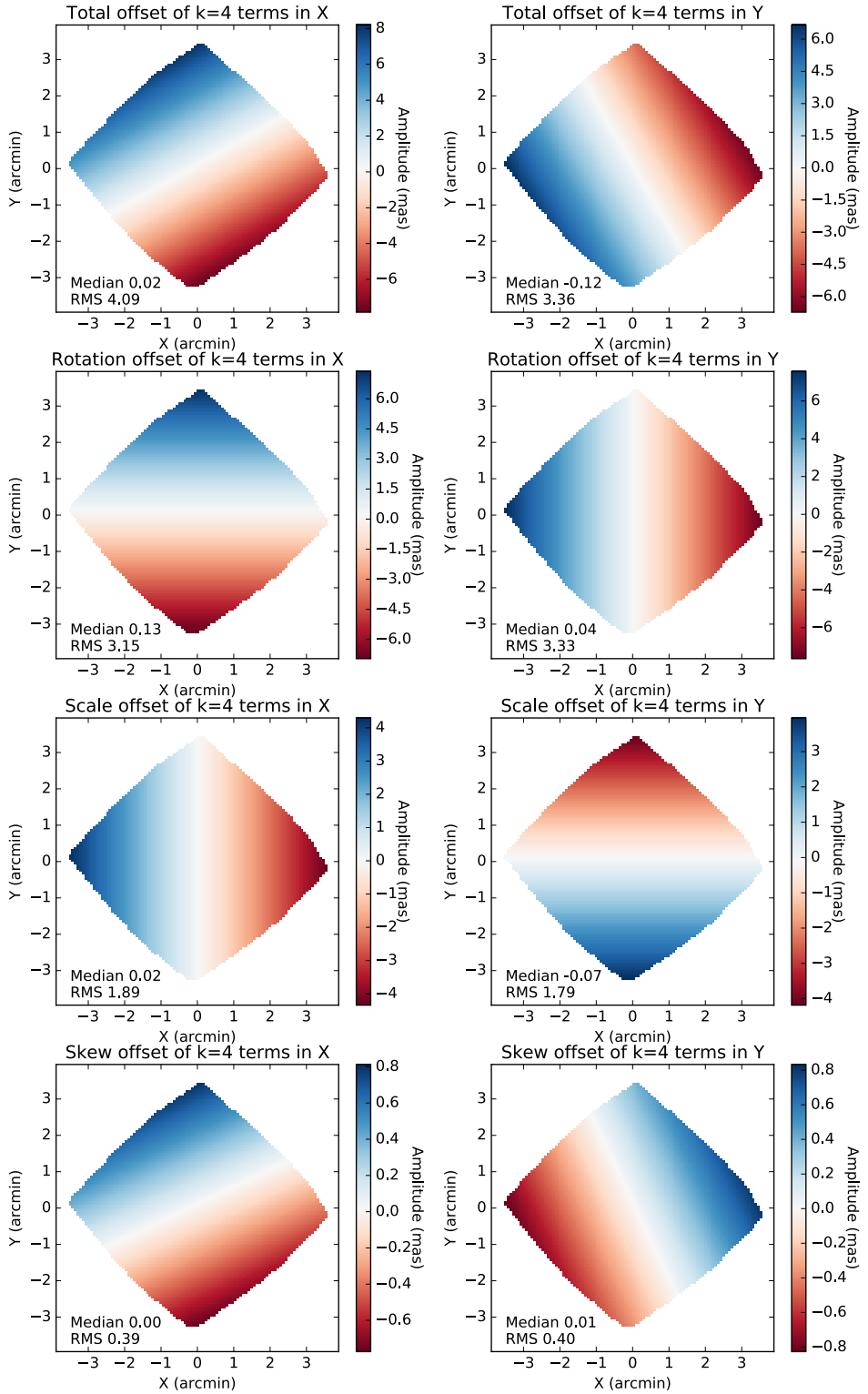

Figure 8: Offsets corresponding to the A_1 and A_2 terms in X (left column) and in Y (right column). The first row shows the total contribution, the second row shows the effect of global rotation, the third row shows the offsets due to the global scale, and the last rows shows the contributions of on-axis skew and off-axis skew. Median and RMS values over the field are reported in each panel and the colorbar indicates extreme values.

5.2.3 Coefficients corresponding to higher-order terms

The field dependence of the offsets corresponding to higher-order terms (k>4, d>1) as inferred from the polynomial solution is shown in Figure 9.

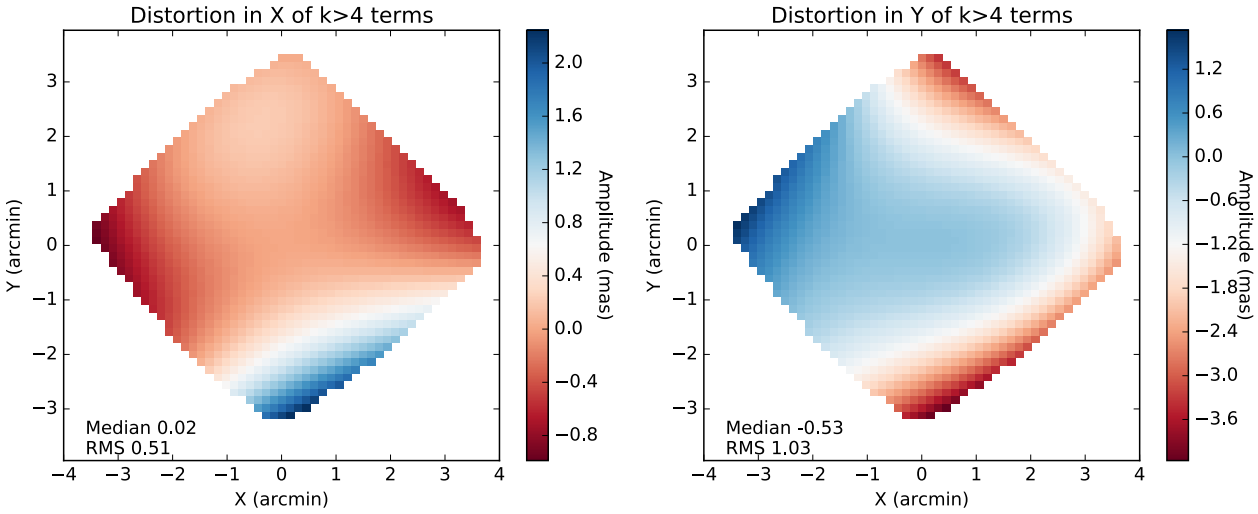

Figure 9: Field dependence of the combined offsets caused by higher-order distortion terms (k=6 and k=8).

5.2.4 Global scale variation across the field

When including higher-order terms, the global scale defined as $\sqrt{bf - ce}$ (Section 5.1) becomes field-dependent because the partial derivatives are no longer constant. At the reference point, the scale of the HST catalog compared to Gaia is 0.999980 ± 0.000001 (see also Table 5). In addition, there is a variation of the global scale across the field that is between –2e-5 and +3e-5, as shown in Figure 10.

Similarly, the global rotation and the on- and off-axis skew terms vary across the field.

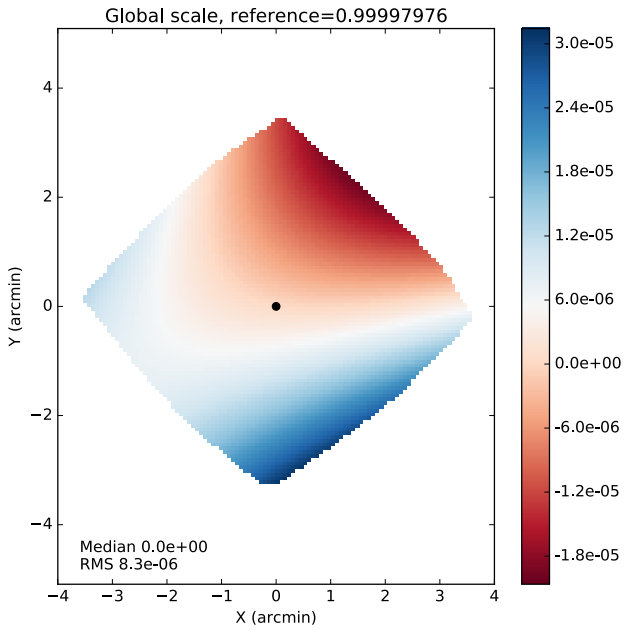

Figure 10: Global scale as a function of field position. The scale at the reference point (black circle) is reported in the title. The colorbar indicates deviation from the reference point scale.

5.2.5 Inverse transformation

We also fitted the k=8 polynomial to derive the mapping from HST (evaluation frame E) to Gaia (reference frame R), using the same set of stars and the polynomial:

$$x_{i,R} - x_{0,R} = {}^{\{x\}}B_0 + \sum_{l=1}^{k/2-1} \sum_{\substack{\alpha,\beta=0,\\ \alpha+\beta=l}}^{l} {}^{\{x\}}B_l^{\alpha,\beta}(x_{i,E} - x_{0,E})^{\alpha}(y_{i,E} - y_{0,E})^{\beta}$$

$$y_{i,R} - y_{0,R} = {}^{\{y\}}B_0 + \sum_{l=1}^{k/2-1} \sum_{\substack{\alpha,\beta=0,\\ \alpha+\beta=l}}^{l} {}^{\{y\}}B_l^{\alpha,\beta}(x_{i,E} - x_{0,E})^{\alpha}(y_{i,E} - y_{0,E})^{\beta}$$

Table 6 and Table 7 show the results. As expected, the offsets change signs and the scale is now larger than unity. Upon inspecting the F-test probabilities, it becomes apparent that the consideration of uncertainties in both dependent and independent variables in the complete solution is important. Applying the same criterion (probability >0.0027) to identify the highest significant mode with the direct solution would lead us to believe that we need a k=12 (d=5) polynomial, whereas the complete solution indicates that the k=8 polynomial is sufficient for the inverse transformation as well. This arises from the asymmetry between nominal and inverse transformation in the direct solution, which considers either uncertainties in Gaia or HST, but not both.

Table 6: Inverse transformation: residuals and F-test probability as a function of polynomial mode

Mode	Degree	Direct solution				Complete solution			
		RMS (mas)		F-test probability		RMS (mas)		F-test probability	
k	*d*	X	Y	X	Y	X	Y	X	Y
4	1	1.841	2.513	2.27e-38	1.72e-80	1.835	2.514	2.22e-24	6.14e-48
6	2	1.805	2.391	2.25e-06	4.50e-14	1.789	2.388	6.41e-03	2.93e-07
8	3	1.803	2.374	1.04e-03	4.28e-07	1.783	2.370	6.40e-02	8.68e-03
10	4	1.798	2.367	1.63e-02	9.92e-05	1.779	2.360	2.18e-01	1.61e-01
12	5	1.798	2.369	3.06e-01	1.84e-01	1.775	2.357	7.20e-01	1.75e-01

Table 7: Inverse transformation: Polynomial coefficients for *k*=8 (degree *d*=3).

		Direct solution				Complete solution			
		X		Y		X		Y	
Reduced chi^2		26.54		8.26		0.70		0.99	
Param	Term	value	sigma	value	sigma	value	sigma	value	sigma
B_0	1	79.778	0.064	-22.742	0.073	79.811	0.088	-22.756	0.094
B_1	x	1.000022	0.000001	0.000032	0.000001	1.000022	0.000001	0.000032	0.000001
B_2	y	-0.000038	0.000001	1.000020	0.000001	-0.000039	0.000001	1.000019	0.000002
B_3	x^2	1.75e-11	3.88e-12	6.47e-12	4.42e-12	1.70e-11	5.24e-12	6.30e-12	5.64e-12
B_4	x*y	4.55e-11	6.39e-12	-1.32e-11	6.88e-12	3.82e-11	8.64e-12	1.57e-12	9.25e-12
B_5	y^2	-3.78e-11	4.02e-12	8.65e-11	4.40e-12	-3.22e-11	5.63e-12	8.80e-11	6.03e-12
B_6	x^3	-1.25e-16	3.72e-17	2.26e-16	4.27e-17	-3.87e-17	5.20e-17	2.13e-16	5.58e-17
B_7	x^2*y	1.08e-16	8.44e-17	-3.35e-16	9.52e-17	1.05e-16	1.17e-16	-2.70e-16	1.25e-16
B_8	x*y^2	-2.18e-16	8.57e-17	6.66e-16	9.52e-17	-2.13e-16	1.22e-16	6.80e-16	1.30e-16
B_9	y^3	1.71e-16	3.98e-17	-1.54e-16	4.42e-17	1.49e-16	5.73e-17	-9.20e-17	6.13e-17

As a validation check, we applied the inverse transformation to the coordinates of the HST catalog to produce a corrected version that is aligned with the Gaia reference frame. We then repeated the crossmatch with the Gaia sources with smaller radius of 0.015 arcseconds, skipped the outlier rejection, and computed *apparent* proper motions (PMs, *apparent* because there may be false identifications), i.e. differences in RA and Dec divided by the time baseline between both catalogs. The *apparent* PMs of 2069 stars are shown in Figure 11, where we chose the same layout as Figure 4 of Anderson & Diaz (2011), i.e. the 88 stars with *apparent* PMs larger than 0.05 HST/ACS pixels over three years are shown with crosses. The majority of PMs are close to zero, as expected, and for high-PM stars there is a strong correlation between the PMs in RA and Dec, which possibly hints towards a systematic origin and not *real* proper motion.

The corrected HST catalog is available at
https://grit.stsci.edu/NIRISS/commissioning_catalog_lmc_calibration_field.

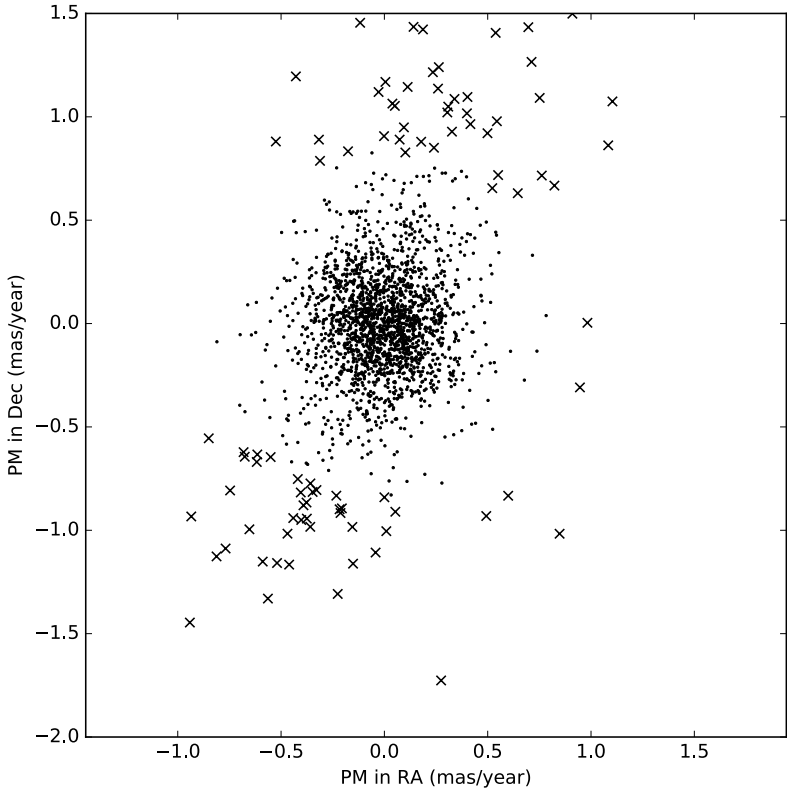

Figure 11: Apparent proper motions of stars that were crossmatched within a 15 mas radius between the corrected HST catalog and the Gaia DR1 catalog.

6 Discussion

6.1 Quality of the Gaia catalog

We have implicitly assumed that the Gaia catalog is accurate and effectively distortion-free in the JWST calibration field, i.e. accurately represents the position, scale, and rotation of the stellar field. Given that DR1 is based on only one year of Gaia observations and several calibrations (e.g. stellar color terms) were not or were only partially applied during its production (Lindegren et al. 2016) we have to be cautious when interpreting our results. Future Gaia data releases will inform us to which extent our assumption was justified.

There are two notable DR1 characteristics of the 2020 sources considered:

1. There are strong correlations between the RA and Dec measurements of individual stars ('ra_dec_corr' field in the Gaia source table) with a mean value of 0.60 and an RMS of 0.2.
2. The median coordinate uncertainty is 0.37 mas in RA and 0.78 mas in Dec, i.e. it is twice as large in Dec, which is also the axis in which we find larger residuals of the distortion fit (residual RMS of 1.8 mas in RA and 2.4 mas in Dec).

However, the extensive DR1 validation effort and the current literature do not indicate significant problems with the absolute or relative astrometry within the quoted uncertainties (Arenou et al. 2017).

6.2 Offsets, rotation, scale, and skew

At its reference epoch J2015.0, the Gaia DR1 positions are aligned with the ICRF to better than 0.1 mas (Lindegren et al. 2016). In contrast, the generation of the HST catalog was not optimized for absolute astrometry and used 2MASS as absolute reference. Consequently, it is not surprising that we find offsets of about –80 mas in RA and +23 mas in Dec that are large compared to the uncertainty in the relative astrometry of 1 to 2 mas.

Given the 8.5 year baseline between the two catalog epochs (~2006.5 for HST and 2015.0 for Gaia) and the LMC proper motion values of van der Marel & Sahlmann (2016), the expected offsets would be –16 mas in RA and –2 mas in Dec.

The global rotation of +7.36 ± 0.20 arcseconds at the reference point of HST relative to Gaia is compatible with the random uncertainty in the ACS orientation of 4.8e-5 radians = 9.9 arcseconds (van der Marel et al. 2007).

The global scale difference between HST and Gaia of 2.0 ± 0.1 e-5 is slightly larger than the expected level of uncertainty in the ACS scale of 1.1e-5 (random) and ≤0.6e-5 (systematic) (van der Marel et al. 2007).

At the edge of the field about 3 arcmin away from the center, this level of rotation and scale difference causes the largest positional offsets of approximately ±7 mas and ±4 mas, respectively, see Figure 8.

We determined skew terms at the reference point of –1.9 ± 1.0e-06 (on-axis skew) and 3.89 ± 0.97e-06 (off-axis skew), comparable and smaller than the uncertainties of 3e-6 (random) and 13e-6 (systematic) reported by van der Marel et al. (2007), respectively.

6.3 Higher-order terms

As evidenced in Table 2 and Figure 4, the polynomial coefficients for $k>4/d>1$ have a significant contribution, i.e. there is significant distortion between the HST and Gaia frames. Quantitatively, the k=6 and k=8 (second and third degree) terms A_3,A_4,A_5, A_6,A_7,A_8,A_9 correspond to offsets with an RMS of 0.51 mas in X and 1.03 mas in Y. The field dependence is shown in Figure 9, which illustrates that offsets are largest at the field edges.

The higher-order terms thus imply corrections that are larger than the relative astrometric accuracy of about 1 mas in the HST catalog (Anderson & Diaz 2011).

To quantify the total contribution of terms that are not global offset, global rotation, or global scale (i.e. distortions in the HST convention), we show Figure 12. The RMS contribution of those skew and higher-order terms is 0.45 mas in X and 0.93 mas in Y, where the RMS in Y is dominated by small regions at the North and South edges of the field. The offset amplitudes remain smaller than 5 mas in all cases.

The total contribution of terms that correspond to field distortions in the convention adopted here, i.e. that are not global offset or global rotation, is shown in Figure 13. The RMS contribution of those scale, skew, and higher-order terms is 2.01 mas in X and 1.66 mas in Y. The offset amplitudes reach extreme values >5 mas in X and >7 mas in Y.

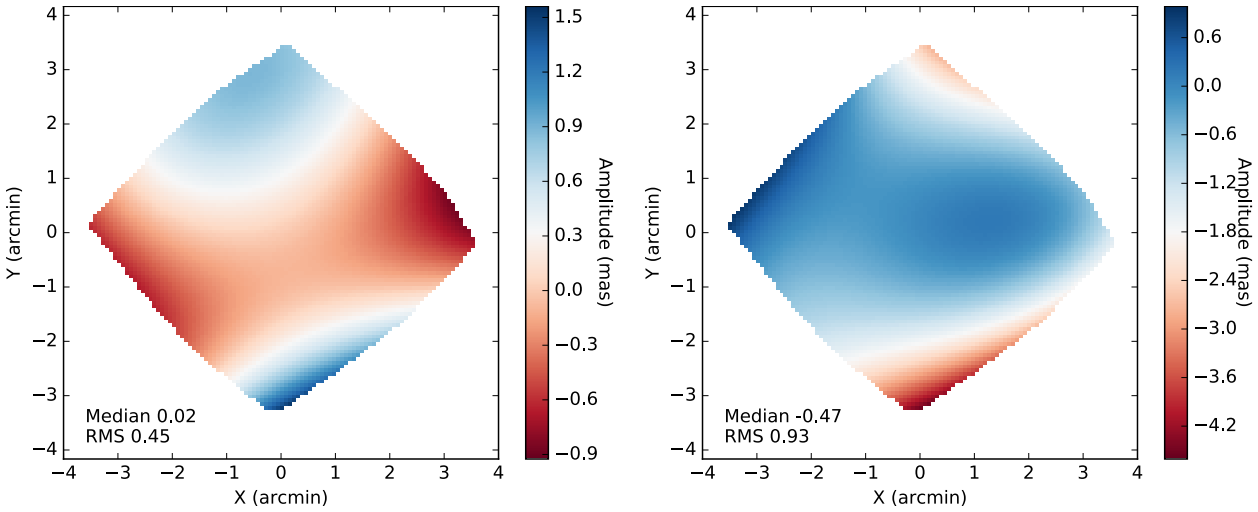

Figure 12: Field dependence of offsets caused by terms that are not global offsets, global rotation, or global scale. This is the combined effect of on-axis skew, off-axis skew, and higher-order terms.

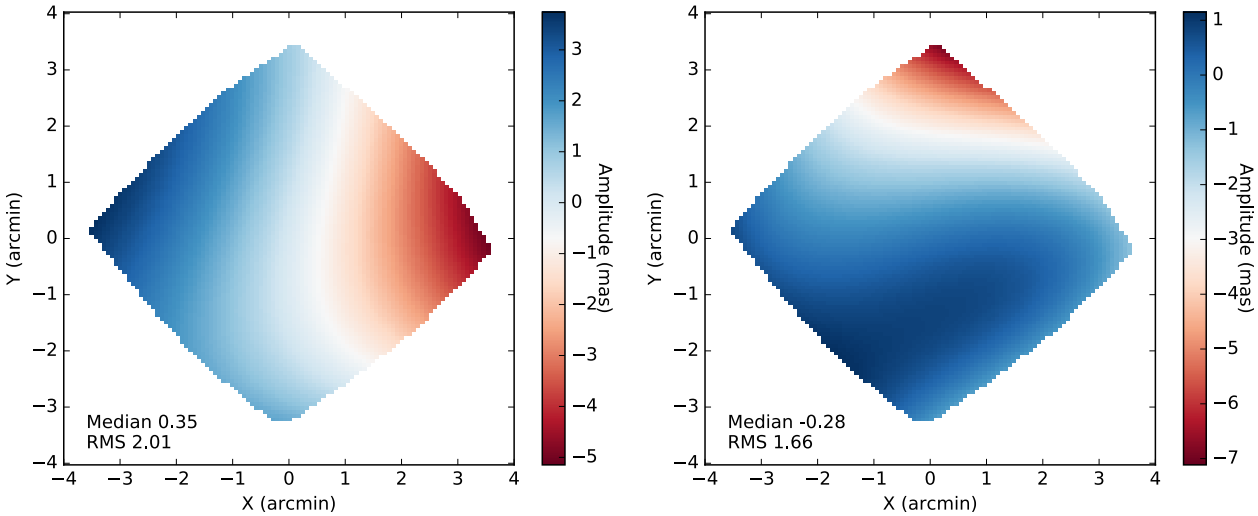

Figure 13: Field dependence of offsets caused by terms that are not global offsets or global rotation. This is the combined effect of global scale, on-axis skew, off-axis skew, and higher-order terms.

6.4 Amplitude of the residuals

Assuming an internal velocity dispersion of 50 km/s and a distance of 50 kpc for stars in the LMC, the PM dispersion in the 8.5 years between the HST and Gaia epochs corresponds to 1.8 mas. This is consistent with the residual dispersion in X (RA) of 1.78 mas but smaller than the dispersion in Y (Dec), which is 2.36 mas. The anisotropy of the residuals is thus 2.36/1.78 = 1.33.

To test for dependence on the considered stellar population, we selected three subsets of stars from the HST catalog:

1. For 1660 crossmatched stars that have measured (not extrapolated) *K*-band photometry (Figure 14), we find a residual dispersion of 1.74 mas in X and 2.27 mas in Y (anisotropy = 1.30).
2. For 1425 crossmatched stars that have *V*-*K* > 1.7, i.e. predominantly the red-giant branch

stars, we find a residual dispersion of 1.78 mas in X and 2.33 mas in Y (anisotropy = 1.31).

3. For 242 crossmatched stars that have V-K < 1.7, i.e. predominantly the younger blue stars, we find a residual dispersion of 1.33 mas in X and 1.70 mas in Y (anisotropy = 1.28).

If we interpret the residual amplitude as a measure of velocity dispersion, the trend goes into the right direction, i.e. young blue stars seem to have a smaller dispersion than older red stars. However, given the amplitude of the effect and the significantly different sample sizes with the uncertainties involved, this test is inconclusive. A more detailed investigation is beyond the scope of this work.

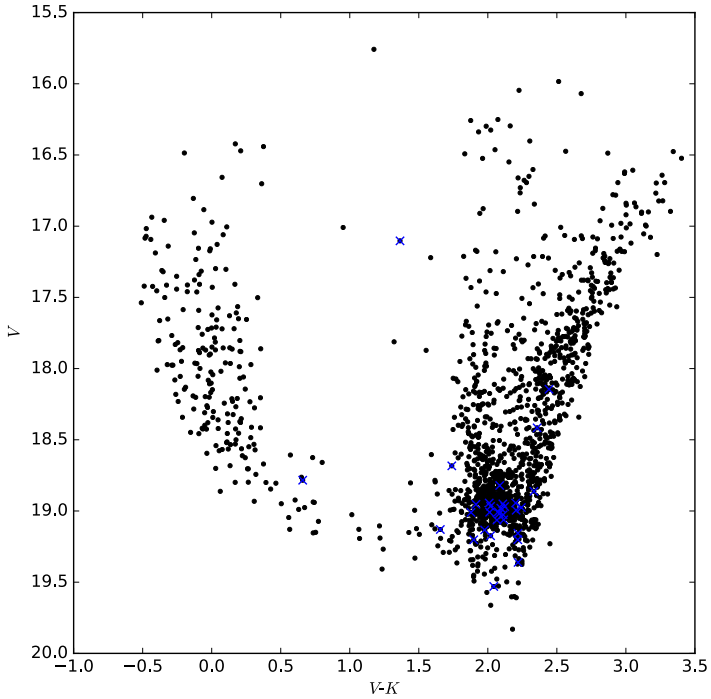

Figure 14: Color-magnitude diagram of 1723 crossmatched stars with measured *K*-band photometry. Blue crosses identify stars with high *apparent* PM in Figure 11.

6.5 Applications of the methods and code

The methods and code for distortion fitting and analysis presented here can be applied to investigate the distortion between any set of positional catalogs. A very similar procedure will have to be followed for the analysis of JWST commissioning observations of astrometric calibration fields to determine the geometric distortion of the imaging science instruments. In particular, the code fulfills the JWST S&OC guideline of being fully written in python and it is operating in a python 3.5 environment.

7 Conclusions

We used the Gaia DR1 to perform verification of the astrometric catalog of the JWST calibration field produced on the basis of HST ACS observations. Under the assumption that the Gaia catalog is accurate and distortion-free, we show that the measured offsets, rotation, scale, and skew between both systems are significant but in general compatible with the known

uncertainties of the ACS astrometric calibration. However, we also identified significant higher-order terms that should be included to map the HST catalog onto the Gaia reference frame, corresponding to large offsets in particular at the field edges.

To facilitate further exploration of these findings we made the crossmatched catalogs and the corrected HST catalog available at https://grit.stsci.edu/NIRISS/commissioning_catalog_lmc_calibration_field.

An informative additional verification would be to perform a representative study of the various well-characterized HST astrometric fields in comparison with the Gaia DR1 data, which requires that there is a sufficient number of $V < 21$ stars in each field. This may potentially also benefit various scientific applications of proper motion measurements derived from the HST data.

This study demonstrates that it will be necessary to incorporate information from the Gaia absolute and relative astrometry in the characterization of the JWST calibration field when that is used to determine the field-distortion of JWST science instruments (i.e. global scale, skew, and higher-order terms) to an accuracy at the level of 2 mas or better.

Given the importance of the JWST calibration field, it is likely that this study will be repeated when the second Gaia data release (DR2) is available or if an additional HST epoch should be obtained.

Since the fit residuals appear to be dominated by internal PM dispersion, performing the same exercise with stars that have measured PM has the potential of decreasing the residuals, thereby increasing the model fidelity for JWST SI distortion calibration. The Gaia DR2 expected in 2018 will provide us with proper motions for a majority of the Gaia stars in the calibration field, which is only a small subset (~2 %) of the HST catalog used here. Acquiring an additional HST epoch of the LMC calibration field can thus yield an improvement by providing PM constraints for virtually all measured stars and importantly for stars that are unlikely to saturate in the JWST calibration images.

8 Acknowledgements

I thank Jay Anderson and Stefano Casertano for insightful discussions and comments on an earlier version of the manuscript. I thank Matt Lallo for pointing out details on the field distortion requirements. All calculations and graphics were made in python3.5. This work made use of astropy, numpy, scipy, matplotlib, ipython, the Kapteyn package (Terlouw & Vogelaar 2015), and of data from the European Space Agency (ESA) mission Gaia (http://www.cosmos.esa.int/gaia), processed by the Gaia Data Processing and Analysis Consortium (DPAC, http://www.cosmos.esa.int/web/gaia/dpac/consortium). Funding for the DPAC has been provided by national institutions, in particular the institutions participating in the Gaia Multilateral Agreement.

9 References

Anderson, J., 2007, Variation of the Distortion Solution of the WFC, Technical Report Instrument Science Report ACS 2007-08, STScI

Anderson, J., 2008, IR Photometry of the JWST Calibration Field, Technical Report JWST-STScI-001378, STScI

Anderson, J., 2016, Verification of Plan to Solve for the Distortion Solution, Technical Report JWST-STScI-005361, STScI

Anderson, J., Diaz, R., 2011, Validation of the Astrometry in the JWST Calibration Field, Technical Report JWST-STScI-002474, STScI

Arenou, F., Luri, X., Babusiaux, C., et al., 2017, ArXiv e-prints

Cox, C., Lallo, M., 2017, Description and Use of the JWST Science Instrument Aperture File, Technical Report JWST-STScI-001550, STScI

Diaz-Miller, R.I., 2007, In: Sterken, C. (ed.) The Future of Photometric, Spectrophotometric and Polarimetric Standardization, vol. 364 of Astronomical Society of the Pacific Conference Series, 81

Gaia Collaboration, Brown, A.G.A., Vallenari, A., et al., 2016a, A&A, 595, A2

Gaia Collaboration, Prusti, T., de Bruijne, J.H.J., et al., 2016b, A&A, 595, A1

Lallo, M., Nelan, E.P., Cox, C., Henry, R., 2016, Verification of Requirements on Pointing Accuracies in JWST Science Products, Technical Report JWST-STScI-004996, STScI

Lazorenko, P.F., Lazorenko, G.A., 2004, A&A, 427, 1127

Lindegren, L., Lammers, U., Bastian, U., et al., 2016, A&A, 595, A4

STScI, 2014, DATA MANAGEMENT SUBSYSTEM REQUIREMENTS DOCUMENT, Technical Report JWST-STScI-002249

STScI, 2016, Science and Operations Center Science and Operations Center Element Requirements Document, Technical Report JWST-STSCI-000046

Terlouw, J.P., Vogelaar, M.G.R., 2015, Kapteyn Package, version 2.3, Kapteyn Astronomical Institute, Groningen, Available from http://www.astro.rug.nl/software/kapteyn/

van der Marel, R.P., Sahlmann, J., 2016, ApJ, 832, L23

van der Marel, R.P., Anderson, J., Cox, C., et al., 2007, Calibration of ACS/WFC Absolute Scale and Rotation for Use in Creation of a JWST Astrometric Reference Field, Technical Report Instrument Science Report ACS 2007-007, STScI